[CANCER RESEARCH 60, 3927–3939, July 15, 2000]

The Role of Cellular Glutathione Peroxidase Redox Regulation in the Suppression of Tumor Cell Growth by Manganese Superoxide Dismutase[1]

Shijun Li, Tao Yan, Ji-Qin Yang, Terry D. Oberley, and Larry W. Oberley[2]

Radiation Research Laboratory, B180 Medical Laboratories, College of Medicine, The University of Iowa, Iowa City, Iowa 52242 [S. L., T. Y. J-Q. Y., L. W. O.]; Pathology Service, William S. Middleton Veterans Memorial Hospital, Madison, Wisconsin 53705 [T. D. O.]; and Department of Pathology and Laboratory Medicine, University of Wisconsin-Madison, Madison, Wisconsin 53705 [T. D. O.]

ABSTRACT

Manganese-containing superoxide dismutase (MnSOD) is an essential primary antioxidant enzyme that converts superoxide radical to hydrogen peroxide and molecular oxygen within the mitochondrial matrix. Cytosolic glutathione peroxidase (GPX) converts hydrogen peroxide into water. MnSOD is reduced in a variety of tumor types and has been proposed to be a new kind of tumor suppressor gene, but the mechanism(s) by which MnSOD suppresses malignancy is unclear. According to the enzymatic reactions catalyzed by MnSOD and cytosolic GPX, change in the cellular redox status, especially change attributable to accumulation of hydrogen peroxide or other hydroperoxides, is a possible reason to explain the suppression of tumor growth observed in MnSOD-overexpressing cells. To test this possible mechanism, we transfected human cytosolic GPX cDNA into human glioma cells overexpressing MnSOD. The results showed that GPX overexpression not only reversed the tumor cell growth inhibition caused by MnSOD overexpression but also altered the cellular contents of total glutathione, reduced glutathione, oxidized glutathione, and intracellular reactive oxygen species. Overexpression of GPX also inhibited degradation of the inhibitory subunit α of nuclear factor-κB. These results suggest that hydrogen peroxide or other hydroperoxides appear to be key reactants in the tumor suppression by MnSOD overexpression, and growth inhibition correlates with the intracellular redox status. This work suggests that manipulations that inhibit peroxide removal should enhance the tumor suppressive effect of MnSOD overexpression.

INTRODUCTION

To protect themselves from oxidative damage, cells have developed a sophisticated antioxidant enzyme defense system (Fig. 1). In this system, SODs[3] convert superoxide radical (O_2^-) into hydrogen peroxide (H_2O_2), whereas GPXs and CATs convert H_2O_2 into water. Therefore, two toxic species, O_2^- and H_2O_2, are converted into the harmless product water. Unlike SOD and CAT, GPX requires several secondary enzymes (GR and G-6-PDH) and cofactors (GSH, NADPH, and glucose 6-phosphate) to function at high efficiency. The relationships between these various proteins and cofactors are shown in Fig. 1.

MnSOD (EC 1.15.1.1) is an essential primary antioxidant enzyme that converts O_2^- to H_2O_2 and O_2 within the mitochondrial matrix. A variety of cancer cells have reduced levels of antioxidant enzymes, especially MnSOD, when compared with their normal counterpart (1). Studies have demonstrated that transfection of *MnSOD* cDNA into various types of tumor cells leads to a decrease in their tumorigenicity (2–7), which suggests that *MnSOD* is a tumor suppressor gene; however, the mechanism(s) by which this antioxidant enzyme suppresses cancer development is currently unclear. The main purpose of the present study was to examine the mechanism of tumor suppression by MnSOD; in particular, we sought to determine the molecular species responsible for the tumor suppression.

Cytosolic GPX (GPX1; EC 1.11.1.9), a selenoprotein, was first described by Mills as an enzyme that protects hemoglobin from oxidative degradation in RBCs (8). There are at least five GPX isoenzymes found in mammals (9). Among them, GPX1 is considered as the major enzyme responsible for removing H_2O_2. Overexpression of this enzyme was observed to protect cells against oxidative damage (10–12). Elevation of GPX1 activity in both FL5 (13) and MDBK cells (14) suppressed apoptosis induced by H_2O_2. This evidence indicates that GPX1 is a major antioxidant enzyme that protects cells against lethal oxidative stress.

It has been suggested that overexpression of SOD without concomitant increase in the level of GPX1 results in the accumulation of H_2O_2 that can participate in the Fenton reaction, leading to the formation of noxious hydroxyl radicals. This highly ROS oxidizes DNA, protein, and lipids, directly affecting cell survival (15, 16). Amstad *et al.* (15) found that the SOD and CAT double transfectant SOCAT 3 was well protected from oxidant damage because of its increased content of CAT, which counterbalances the increase in CuZnSOD. Furthermore, they reported that GPX1 also compensated for the hypersensitivity of CuZnSOD overproducers to oxidant stress (17). This evidence implied that the balance of SOD and GPX plus CAT is more important to overall oxidant sensitivity than the level of SOD alone.

Redox (reduction-oxidation) reactions regulate signal transduction (18–22). H_2O_2, O_2^-, GSH/GSSG, and NADPH/$NADP^+$ are considered to be important players in the cellular redox system. The GSH/GSSG couple is thought to be the major redox buffer in the cell (23, 24). As shown in Fig. 1, GPX1, in addition to affecting GSH/GSSG, controls the cellular content of H_2O_2 (or other organic hydroperoxides) and NADPH/$NADP^+$, so it may regulate the cellular redox status. In HIV-infected T-cells (25) and similarly in T-cell lines (26), selenium supplementation increased GPX activity and decreased H_2O_2-induced NF-κB activation. A human breast cancer cell line (T47D) overexpressing GPX1 responded poorly to NF-κB activation by TNF-α or H_2O_2; both κB-dependent gene transactivation and NF-κB DNA binding were reduced (27).

In this paper, we hypothesize that overexpression of MnSOD in human glioma cells results in an accumulation of H_2O_2 or other peroxides, causing a decrease in glioma cell growth. Furthermore, we hypothesize that transfection of these cells with the human *GPX1* gene will rescue the growth of these cells through detoxification of hydrogen peroxide or hydroperoxides and/or changes in cellular redox status. To test our hypotheses, we transfected the human *GPX1* cDNA into human glioma MnSOD-overexpressing cells. The results indicate that overexpression of GPX1 rescues the growth suppression by MnSOD, which suggests that H_2O_2 or some other hydroperoxide is

Received 10/20/99; accepted 5/16/00.

The costs of publication of this article were defrayed in part by the payment of page charges. This article must therefore be hereby marked *advertisement* in accordance with 18 U.S.C. Section 1734 solely to indicate this fact.

[1] This research was supported by NIH Grant CA 66081 (to L. W. O.) and by the Department of Veterans Affairs Research Service (to T. D. O.).

[2] To whom requests for reprints should be addressed. Phone: (319) 335-8015; Fax: (319) 335-8039; E-mail: larry-oberley@uiowa.edu.

[3] The abbreviations used are: SOD, superoxide dismutase; CAT, catalase; CuZnSOD, copper-and zinc-containing SOD; DCFH, 2′,7′-dichlorodihydrofluorescein; DCFH-DA, DCFH diacetate; ddH_2O, double-distilled water; DTNB, 5,5′-dithiobis(2-nitrobenzoic acid); G-6-PDH, glucose-6-phosphate dehydrogenase; GPX, glutathione peroxidase; GR, glutathione reductase; GSH, reduced glutathione; GSSG, glutathione disulfide; IκB_α, inhibitory subunit α of NF-κB; MnSOD, manganese-containing SOD; NF-κB, nuclear factor-κB; P, parental; ROS, reactive oxygen species; RT, reverse transcription; TNB, 5-thio-2-nitrobenzoic acid; TNF-α, tumor necrosis factor α.

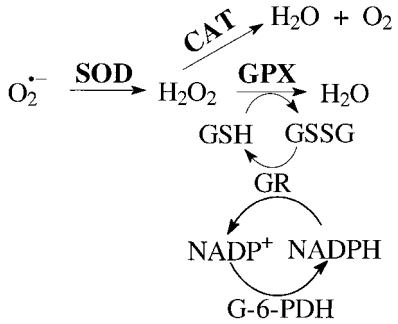

Fig. 1. Antioxidant enzyme system. The SODs convert superoxide radical into hydrogen peroxide. The CATs and GPXs convert hydrogen peroxide into water. In this way, two toxic species, superoxide radical and hydrogen peroxide, are converted into the harmless product water. GPX requires several secondary enzymes (GR and G-6-PDH) and cofactors (GSH, NADPH, and glucose 6-phosphate) to function. In this scheme, GR and G-6-PDH are considered secondary antioxidant enzymes, because they do not act on ROS directly but enable GPX to function.

involved in the cell growth suppression. It is uncertain whether H_2O_2 increases after SOD overexpression or whether, instead, other hydroperoxides increase. Omar and McCord (28) have postulated that increased SOD does not cause an increase in H_2O_2, but instead an increase in lipid hydroperoxides. GPX1 can act on both H_2O_2 and lipid hydroperoxides, so it is not clear which hydroperoxide is being acted on by GPX1. We also found that overexpression of GPX1 alters the cellular contents of GSSG, ratios of GSH/GSSG, and levels of ROS and inhibits $I\kappa B_\alpha$ degradation, which suggests that GPX1 can modulate the intracellular redox status. Immunogold ultrastructural staining showed that GPX1 protein exists in the mitochondria and nucleus, as well as in the cytosol. Thus, GPX1 protein overexpression may remove hydroperoxides produced by MnSOD in the mitochondria.

MATERIALS AND METHODS

Materials. 60-mm plastic tissue culture dishes were obtained from Corning. DMEM, high glucose (4.5 g/liter), Geneticin (G418), and LipofectAMINE were purchased from Life Technologies, Inc. (Gaithersburg, MD). Fetal bovine serum was bought from HyClone. Zeocin and plasmid pcDNA3.1/Zeo(+) were obtained from Invitrogen. GR, GSH, and NADPH were from Sigma Chemical Co. $I\kappa B_\alpha$ primary antibody was purchased from New England Biolabs, Inc. CAT primary antibody was from Calbiochem-Novabiochem Corp. (CAB). Blocking Reagent®, Anti-Digoxigenin-AP®, and CSPD® were purchased from Roche Molecular Biochemicals. Primary antibodies against MnSOD, CuZnSOD, and GPX1 were raised by our laboratory. Human *GPX1* cDNA was a gift from Dr. James H. Doroshow.

Cell Lines. The human glioma P U118–9 cells were cloned from wild-type U118 cells (5). Neo is a vector control line that serves as the MnSOD single transfection control and SOD2 is a MnSOD overexpression transfectant. Both Neo and SOD2 were derived from the P cell line by transfection and cloning. SOD2 had been shown previously to have about a 5-fold increase in MnSOD compared to the P cell line (5). These cell lines have been described in detail previously (5). Zeo35 is also a vector control line that serves as MnSOD-GPX1 double transfection control. S-GPXs are MnSOD-GPX1 double transfectants. The Zeo35 and S-GPX cell lines were derived from SOD2 by transfection and cloning. Thus, the lineages of these lines are as follows.

$$\begin{array}{ccccccc} \text{U118} & \rightarrow & \text{U118-9} & \rightarrow & \text{SOD2} & \rightarrow & \text{S-GPXs} \\ & & \downarrow & & \downarrow & & \\ & & \text{Neo} & & \text{Zeo35} & & \end{array} \qquad \text{(A)}$$

Cell Culture. P cells were routinely grown on 60-mm plastic tissue culture dishes in DMEM high-glucose medium supplemented with 10% fetal bovine serum and 1% penicillin/streptomycin at 37°C in a humidified atmosphere of 95% air and 5% CO_2. Medium was changed every 4 days, and the cells were subcultured with 0.25% trypsin and 1% EDTA whenever the cultures reached confluence. Passage numbers were limited to 30 passages, because it has been demonstrated that antioxidant enzymes did not change in tumor cells up to 50 passages (29). Both Neo and SOD2 cells were cultured in medium containing G418 (500 mg/liter). Both Zeo35 cells and S-GPX cells were cultured in medium containing G418 (500 mg/liter) and zeocin (100 mg/liter). To eliminate the influence of antibiotics on experimental results, 3–5 days before an analysis, cells were cultured in medium without any antibiotic supplement. In all assays of our study, the cells were cultured in medium containing 60 nM selenium. Cells were regularly examined for *Mycoplasma* contamination and used only if *Mycoplasma*-free.

Construction of Expression Vector. We synthesized the 89-mer polynucleotides 5′-*CATCCC*AAGCTTACAGTGCTTGTTCGGGGCGCTCGGCTGGCTTCTTGGACAATTGCGCC**ATG**TGTGCTGCTCGGCTAGC*TAGTAGTAGC*-3′ and its complementary strand. This synthesized DNA fragment contained two restriction enzyme sites, *Hin*dIII and *Nhe*I (shown underlined). The nucleotides between the two sites are the same sequence, corresponding to 48 nucleotides of the 5′-noncoding region and 20 nucleotides of the coding region from the ATG start codon of the published human *GPX1* cDNA sequence (30). There is also a *Nhe*I site at nucleotide 20 from the ATG start codon in the *GPX1* cDNA. We annealed the two 89-mer polynucleotide strands, and then this DNA fragment was cut with *Hin*dIII and *Nhe*I. *GPX1* cDNA was cut with *Nhe*I and *Bam*HI. The plasmid [pcDNA3.1/Zeo(+)] was cut with *Hin*dIII and *Bam*HI. Finally, the three enzyme-digested fragments were ligated by T4 DNA ligase. We designated this new construct pcDNA3.1/Zeo(+)/GPX1. The new construct has 41 more nucleotides in the 5′-noncoding region of *GPX1* cDNA than the original *GPX1* cDNA from Dr. Doroshow, which has only 5 nucleotides in the 5′-noncoding region; we constructed this new plasmid because we had difficulty in using the original plasmid for *GPX1* transfection in our cell lines. The construction was confirmed by DNA sequencing by the University of Iowa DNA Facility.

Cell Transfection. The SOD2 cells were transfected with the pcDNA3.1/Zeo (+)/GPX1 plasmid. Zeocin was the selection marker for the transfection. The transfection of vector control was performed by using the plasmid pcDNA 3.1/Zeo(+) without the *GPX1* cDNA insert. The LipofectAMINE method was used in this study. The protocol for transfection with LipofectAMINE as recommended by the manufacturer (Life Technologies) was used with some modification. Cells were seeded at a density of 5×10^5 cells/well in 6-well plates, allowed to grow overnight, and then rinsed three times with serum-free medium before the transfection. The transfection solution was prepared by diluting 2 μg of plasmid DNA into 100 μl of serum-free medium to make solution A and diluting 10 μl of LipofectAMINE into 100 μl of serum-free medium to make solution B. The two solutions were combined, mixed gently, and incubated at room temperature for 45 min to allow DNA-liposome complex formation. Finally, for each transfection, 0.8 ml of serum-free medium was added to the tube containing 200 μl of DNA-liposome complexes, mixed gently, overlaid onto the rinsed cells, and then incubated with the cells for 24 h at 37°C. After transfection, the DNA-lipid complexes were removed and replaced with the fresh medium without supplement of G418 and zeocin. Forty-eight h later, the cells were subcultured and subsequently incubated in the selection medium (500 mg/liter G418 and 100 mg/liter zeocin) for 15 days to allow antibiotic-resistant colony growth. Resistant colonies were isolated by cloning rings.

Cell Homogenization and Protein Quantification. To prevent antioxidant enzyme denaturation, all of the procedures for cell sample preparation were performed on ice. The culture medium was removed before cell harvesting, and the cells were washed with PBS (pH 7.0) three times. Cells then were removed from the dish using a plastic scraper and collected into a microcentrifuge tube. The harvested cells were pelleted by centrifugation, and then the PBS supernatant was removed. The cell pellets were resuspended in 0.05 M phosphate buffer (pH 7.8) and sonicated three times for 15 s each using a Vibra cell sonicator (Sonics and Materials, Inc., Danbury, CT) at full power and 40% duty cycle. Total protein concentrations were measured with the Bio-Rad protein assay kit.

GPX Activity Assay. GPX activity were measured as described by Lawrence and Burk (31). Cell sonicated samples (700 μg/100 μl) were incubated in 0.7 ml of a mixture containing 50 mM potassium phosphate buffer (pH 7.8), 1 mM EDTA, 1 mM NaN_3 10 mM GSH, and 2.4 units/ml GR for 10 min. After addition of 100 μl of 1.5 mM of NADPH, NADPH oxidation was determined

at 340 nm for 3 min at 30 s intervals, which is the independent sample as a reference. NADPH oxidation was then measured after addition of 100 μl of 1.5 mM H_2O_2 at 340 nm for 3 min. One unit of GPX activity is defined as the amount of protein that oxidized 1 μM NADPH per min. It should be emphasized that this assay is run with high GSH levels and measures the GPX activity at that high GSH level. If the cell has low GSH levels, the actual GPX activity will then be lower than measured by this assay. One cannot use low GSH levels in this assay because the activity will then be too small to measure. For this reason, we defined "effective GPX activity" as measured GPX activity times cellular GSH concentration.

Native Activity Gel Assay for GPX1 and GR. Before loading the samples, the gel was run in preelectrophoresis buffer (22.76 g/liter Tris-HCl, 0.38 g/liter disodium EDTA, pH 8.8) for 1 h at 4°C. For GPX1 native activity gel assay, 700 μg of total protein were separated in an 8.0% native polyacrylamide gel with 5% stacking gel. The electrophoresis process was performed in two steps: the gel with samples was run first for 3 h in the preelectrophoresis buffer at 4°, and then run in the sample running electrophoresis buffer (6.06 g/liter Tris-HCl, 22.50 g/liter glycine, 0.68 g/liter disodium EDTA, pH 8.3) for 4 h at 4°C. After electrophoresis, the gel was rinsed with 1 mM GSH three times for 7 min each and then incubated in 75 ml of ddH_2O containing 0.008% cumene hydroperoxide plus 1 mM GSH for 10 min with gently shaking. After briefly rinsing twice with ddH_2O, the gel was stained with a 1% ferric chloride and a 1% potassium ferricyanide solution, which was made fresh and mixed immediately before use from equal volumes of a 2% stock solution of each. The achromatic band corresponding to GPX activity appears on a blue background. For native activity gel assay for GR, 500 μg of total protein were separated in a 7.0% native polyacrylamide gel with 5% stacking gel. The process of electrophoresis was the same as native gel assay for GPX1. After electrophoresis, the gel was placed in a freshly made dye solution [3.4 mM GSSG, 0.36 mM NADPH, 0.052 mM dichlorophenol-indophenol, 1.1 mM 3 (4,5-dimethythiazolyl-2)-2,5-diphenyl tetrazolium acid, prepared in 250 mM Tris, pH 8.0]. GR activity was indicated by the presence of a purple precipitate in the gel. The gel was rinsed repeatedly and photographed.

Western Blotting Assay. The method used for Western blotting assay was described previously (32) and modified. Sample preparation for Western blotting was the same as that of enzyme activity assays. After proteins were electrotransferred onto a nitrocellulose membrane (Schleicher & Schuell, Keene, NH), the membrane was blocked in 5% dry fat-free milk in TBST (0.02 M Tris-HCl buffer, pH 7.5, 0.137 M NaCl, and 0.1% Tween 20) for 1 h at room temperature and probed with primary antibody overnight at 4°C. The MnSOD primary antibody raised in our laboratory was diluted 1:1000, the CuZnSOD primary antibody was diluted 1:250, the CAT primary antibody was diluted 1:1000, and the $I\kappa B_\alpha$ primary antibody was diluted 1:2000. After the immunoreaction with primary antibody, the membrane was incubated with horseradish peroxidase conjugated with goat antirabbit (Sigma) IgG (1:10000) for 1 h at room temperature. After a final wash of the membrane with TBST, the bands were revealed in films by ECL staining (Amersham Pharmacia Biotech). Densitometry was performed by the Eagle Eye II still video system (Stratagene, La Jolla, CA).

Native Immunoblotting Assay. We developed an immunoblotting method to determine the GPX1 protein levels in different clones. The protein separation method was the same as for the GPX activity gel assay. The native proteins were transferred onto the nitrocellulose membrane using the same method as in the Western blotting assay. The detection method is also the same as that for the Western blotting. The GPX1 primary antibody was diluted 1:100.

Northern Blotting. The total RNA were extracted from 80−90% confluent cells using a RNeasy Mini Kit according to the manufacturer's directions (Qiagen). Twenty μg of the total RNA were resolved in a 1.5% agarose gel [0.75 g of agarose, 42.2 ml of ddH_2O, 5 ml of 10× 3-(*N*-morpholino)propanesulfonic acid (200 mM morpholinopropanesulfonic acid, 50 mM sodium acetate, 10 mM EDTA, pH 7.0), and 2.5 ml of formaldehyde] and then transferred and fixed onto a nylon membrane (Roche Molecular Biochemicals, Indianapolis, IN). The human *GPX1* cDNA were labeled with digoxigenin (Roche Molecular Biochemicals) by the random-priming technique. Prehybridization was performed in the standard hybridization buffer [5× SSC (0.75 M NaCl, 0.75 M sodium citrate, pH 7.8), 0.1% *N*-lauroylsarcosine, 0.02% SDS, 1% Blocking Reagent®] for at least 4 h at 68°C. Hybridization was carried out in the same standard hybridization buffer as prehybridization containing a human *GPX1* cDNA probe overnight at 68°C. After hybridization, the membrane was washed twice, 15 min per wash, in 2× wash solution [2× SSC (0.3 M NaCl, 0.3 M sodium citrate, pH 7.8), 0.1% SDS] at room temperature and then twice with 0.5× wash solution [0.5× SSC (75 mM NaCl, 75 mM sodium citrate, pH 7.8), 0.1% SDS], 15 min per wash, at 68°C. After the posthybridization washes, the membrane was equilibrated in the washing buffer [maleic acid buffer (0.1 M maleic acid, 0.15 M NaCl, pH 7.5), 0.3% (v/v) Tween 20] for 1 min, and then the membrane was blocked by gentle agitation in the blocking solution (dilute Blocking Reagent® stock solution 1:10 with maleic acid buffer) for 1 h at room temperature. After pouring off the blocking solution, the membrane was incubated in the antibody solution Anti-Digoxigenin-AP®; blocking solution, 1:10,000) for 30 min at room temperature. After discarding the antibody solution, the membrane was washed gently twice, 15 min per wash, in washing buffer. Finally, the detection of the membrane was performed with CSPD® diluted 1:100 in detection buffer (100 mM Tris-HCl, pH 9.5, 100 mM NaCl) according to the instructions provided by the manufacturer (Roche Molecular Biochemicals). Ethidium bromide-stained bands from both 18S (~2 kb) and 28S (~5 kb) rRNA bands served as markers for RNA sample loading.

RT-PCR. The total RNA was isolated as described in the Northern blotting assay. RT of cDNA was carried out from 5 μg of total RNA in a 30-μl reaction solution [2 μg of oligo(dT) (18-mers), 2 μl of 10 mM dNTP (mixture of dATP, dGTP, dTTP, and dCTP), 3 μl of 100 mM DTT, 1 μl of RNase inhibitor (RNasin), 0.3 μl of BSA (100×), 1.5 μl of Moloney murine leukemia virus-reverse transcriptase (200 units/μl), 6 μl of 5× first strand buffer (50 mM Tris-HCl, pH 8.5, 3 mM $MgCl_2$, 75 mM KCl, 10 mM DTT)]. The mixture was incubated to synthesize cDNA for 50 min at 42°C, to elongate cDNA for 10 min at 52°C, and then to inactivate the enzyme for 15 min at 70°C.

PCR primers were selected according to the human complete *GPX1* cDNA sequence. The sequences of oligonucleotide primers were as follows: sense, 5′-AAGGTACTACTTATCGAGAATGTG-3′; antisense, 5′-GTCAGGCTCGATGTCAATGGTCTG-3′. The PCR product was approximately 0.5 kb long. The PCR for one reaction was carried out in a 20-μl mixture [2 μl of 10× PCR buffer, 0.5 μl of 10 mM deoxynucleotide triphosphate (mixture of dATP, dGTP, dCTP, and dTTP), 0.2 μl of 5 units/μl Taq DNA polymerase, 2 μl of cDNA (dilution of RT products, 1:100), 0.1 μl of 1 μg/μl sense primer, 0.1 μl of 1 μg/μl antisense primer, 15.1 μl of ddH_2O)]. PCR was conducted in a Perkin-Elmer Cetus thermal cycler for 30 cycles. After a 5-min denaturation at 94°C, amplification was carried out with a cycling profile consisting of denaturation for 40 s at 94°C, annealing for 40 s at 55°C, and extension for 1 min at 72°C, followed by a final extension for 7 min at 72°C. Fifteen μl of PCR products were resolved in a 1.2% agarose gel with ethidium bromide staining and compared with 1-kb DNA ladders.

Immunogold Staining. Cells were scraped from tissue culture dishes, fixed in Carson-Millonig's fixative (4% formaldehyde in 0.16 M monobasic phosphate buffer, pH 7.2) and processed for immunogold immunohistochemistry as described previously (33). Cell cultures stained with anti-GPX1 antibody were photographed using a Hitachi electron microscope (Hitachi, Ltd., Tokyo, Japan). As a control, normal rabbit serum was used in place of the primary antibody.

Plating Efficiency. A single cell suspension was plated at 500 cells/dish in 60-mm dishes for each clone. The cells were kept in culture medium in an incubator for 14 days to allow colony formation and then fixed and stained by 0.1% crystal violet and 2.1% citric acid. The colonies containing 50 cells or more were scored. The plating efficiency (PE) was calculated as follows: PE = (Colonies formed/Cells seeded) × 100%.

Growth Curve. The growth rate of cells was determined by counting the number of cells as a function of time. Cells were seeded in 24-well plates at 2×10^4 cells/well containing 1 ml of culture medium. Three parallel wells for each clone were seeded for each time point. Cells were counted every 48 h for 12 days using a hemocytometer. Doubling time (T_d) was calculated from the growth curve by using the formula $T_d = 0.693t/\ln(N_t/N_0)$, where t is time in hours, N_t is the cell number at time t, and N_0 is the cell number at the initial time.

Tumorigenicity in Nude Mice. Four- to 5-week-old female nude mice were used in this assay. Cells were harvested by trypsinization and washed in serum-free medium. Twenty million cells of each clone were resuspended in serum-free medium. Two million cells were injected s.c. into the back of the neck of each nude mouse. Four nude mice were used for each group. When the tumor appeared, it was measured by a vernier caliper every week. Tumor

volume (TV) was calculated as follows (34), TV (mm^3) = ($L \times W^2$)/2, where L is the longest dimension of the tumor in mm, and W is the shortest dimension of the tumor in mm.

GSH and GSSG Measurement. The method for GSH and GSSG measurement is adapted from Anderson (35). The total glutathione of cells was measured by the colorimetric reaction of DTNB with GSH to form TNB. The rate of the formation of TNB, which is proportional to the total GSH concentration, was followed spectrophotometrically at 412 nm. Cellular GSSG was reduced to GSH by specific GR. To prepare a sample for total glutathione measurement, the cell pellet was frozen and thawed once, then homogenized in 50 mM potassium phosphate buffer containing 1.34 mM diethylenetriaminepentaacetic acid (to give a protein concentration of 2–10 mg/ml) by running the mixture up and down in the tip of a P-1000 Pipetman. For the total glutathione measurement, the sample was diluted with 5-sulfosalicylic acid (5%, w/v, in ddH_2O) to yield values that fall on the standard curve (usually between 1:2 and 1:10). The total glutathione was determined by mixing 700 μl of working buffer [6 mM NADPH in stock buffer (0.143 M sodium phosphate, 6.3 mM EDTA)], 100 μl of DTNB (6 mM DTNB in stock buffer), 100 μl of ddH_2O, 50 μl of sample, 50 μl of GR (40 units/ml) at room temperature. The rate of TNB formation was determined at 412 nm, every 20 s for 3 min using a Beckman DU-70 spectrophotometer. The total glutathione of a sample was calculated from a standard curve of the concentration of glutathione *versus* rate. For the GSSG measurement, 30–50 μl of homogenate were taken, 2 μl of 2-vinypyridine in 100% of ethanol (1:1) were added, and the sample was vortexed and incubated at 4°C for 1.5 h to remove GSH. The GSSG was measured as described in the total glutathione measurement. The GSH content was calculated by subtracting the GSSG content from the total glutathione content. Because GSH is a derived quantity, errors for GSH were calculated by propagation of error theory.

Intracellular ROS Measurement. The level of intracellular ROS was determined by a microplate reader (Bio-Tek Instruments, Inc., Winooski, VT) using DCFH-DA (Molecular Probes Inc., Eugene, OR; Ref. 36). DCFH-DA is a nonpolar and nonfluorescent compound that can permeate cells freely. Once inside cells, it is hydrolyzed by esterase to form the polar and nonfluorescent DCFH, and trapped inside cells. Upon interaction of DCFH with ROS, DCFH gives rise to cellular fluorescence. Cells (2×10^5 from each clone) were seeded and cultured for 24 h in a 24-well dish prior to the measurement. On the day of assay, the cells were washed twice with serum-free medium and then incubated with 0.5 ml of serum-free medium containing a 30 μM DCFH-DA solution for 90 min at 37°C. After the incubation, the cells were washed twice with PBS buffer (pH 7.8) and then lysed in 0.5 ml of 0.5% SDS solution. Finally, the intensity of the 485/530 nm fluorescence corresponding to the levels of intracellular ROS in the lysates were recorded with a microplate reader (Bio-Tek Instruments, Inc.) using FL500 software. The relative fluorescence was calculated by the equation,

$$\text{Relative fluorescence}/10^4 \text{ cells} = \frac{(\text{Reading of the cells treated with DCFH-DA} - \text{reading of blank})}{\text{Cell number}} \quad \text{(B)}$$

where the blank contained cells in medium without DCFH-DA.

To test for differences in endogenous esterase activity, the already oxidized probe (Molecular Probes C369), which fluoresces without ROS reaction, was also tested. The results were similar among all of the cell lines and indicated no significant difference in esterase activity (data not shown).

Statistics. Both Student's *t* test and the ANOVA-Tukey test were used in the comparison of different groups. The null hypothesis was rejected at the 0.05 level of significance. Linear regression analysis was performed with SigmaPlot 5.0 software. All assays of Western blots, Northern blots, RT-PCR, and activity gels were done at least twice.

RESULTS

Expression of the Human GPX1 Gene in Transfectants. To test our hypothesis, we constructed human *GPX1* cDNA into the pcDNA3.1/Zeo(+) plasmid between the *Bam*HI and *Hin*dIII restriction enzyme sites and then transfected the plasmid into human glioma cells that already overexpressed MnSOD (SOD2). The Zeo35 clone served as vector control to determine the effect of the transfection process and selection pressure on cell growth. Clones that survived under zeocin (100 mg/liter) and G418 (500 mg/liter) were screened by native immunoblotting. Our primary GPX1 antibody does not recognize monomer GPX1 protein using regular Western blotting (32). For analysis of immunoreactive proteins, we therefore used a native immunoblot technique instead of the regular Western blotting method. The expression of the *GPX1* gene at the protein level was measured by native immunoblotting using antibovine GPX1 antiserum, which was specific to native GPX1 protein. Five clones (S-GPX70, S-GPX86, S-GPX146, S-GPX182, and S-GPX220) with high levels of GPX1 protein were selected, and three (S-GPX70, S-GPX86, and S-GPX146) of them were analyzed in all additional studies. The results (shown in Fig. 2*a*) demonstrated that the immunoreactive protein levels of GPX1 were higher in all GPX transfectants compared with SOD2 cells and Zeo35 cells.

To test whether the increased GPX1 protein resulted from the expression of the exogenous cDNA, Northern blotting was carried out using a digoxigenin-labeled *GPX1* cDNA probe. Northern blotting

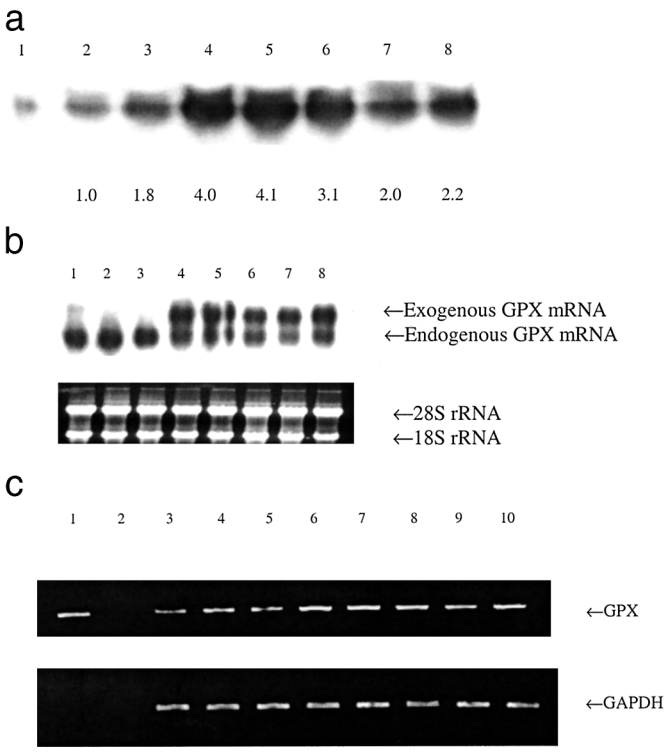

Fig. 2. Examination of GPX1 expression at the mRNA and protein level. *a*, native immunoblotting for GPX1. *Lane 1*, pure bovine GPX1 standard; *Lane 2*, SOD2; *Lane 3*, Zeo35; *Lane 4*, S-GPX70; *Lane 5*, S-GPX86; *Lane 6*, S-GPX146; *Lane 7*, S-GPX182; *Lane 8*, S-GPX220. Results from densitometric analysis are shown *under* each lane; the fold increase relative to cell line SOD2 is given. GPX1 transfectants showed increased amounts of immunoreactive protein. *b*, Northern blotting assay for GPX1. *Lane 1*, Neo; *Lane 2*, SOD2; *Lane 3*, Zeo35; *Lane 4*, S-GPX70; *Lane 5*, S-GPX86; *Lane 6*, S-GPX146; *Lane 7*, S-GPX182; *Lane 8*, S-GPX220. Twenty micrograms of the total RNA were separated on a 1.5% agarose RNA gel. Both 18 S (~2 kb) and 28 S (~5 kb) rRNA bands were visualized to confirm equal sample loading. There were new bands in GPX transfectants, indicating expression from the exogenous plasmid. *c*, detection of GPX1 mRNA by RT-PCR. *Lane 1*, positive control; *Lane 2*, negative control; *Lane 3*, Neo; *Lane 4*, SOD2; *Lane 5*, Zeo35; *Lane 6*, S-GPX70; *Lane 7*, S-GPX86; *Lane 8*, S-GPX146; *Lane 9*, S-GPX182; *Lane 10*, S-GPX220. cDNA synthesis was carried out from 5 μg of total RNA in a 30-μl reaction solution. 2 μl of cDNA (dilution of RT products at 1:100) was amplified in a 20-μl PCR mixture for 30 cycles. Fifteen microliters of PCR products (0.5 kb) were separated in a 1.2% agarose gel with ethidium bromide staining and compared with 1-kb DNA ladders. The brightest bands were found in GPX1 transfectants. *GAPDH*, glyceraldehyde-3-phosphate dehydrogenase.

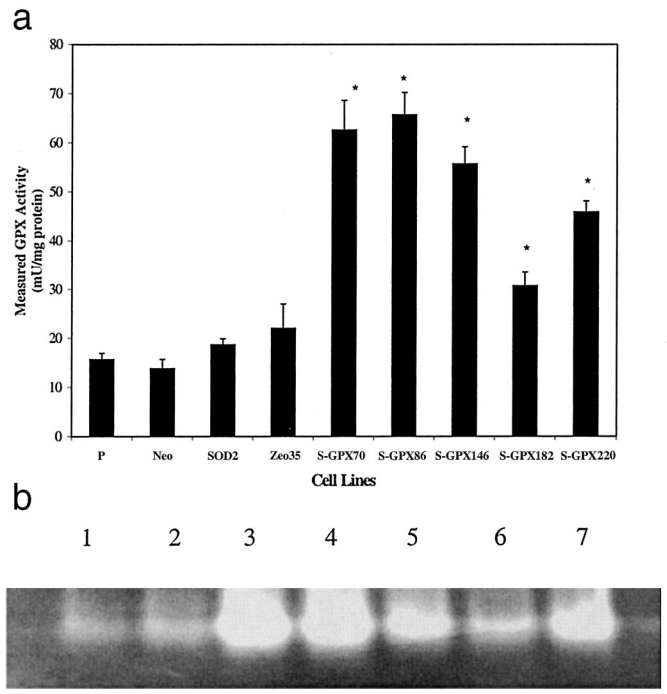

Fig. 3. Examination of GPX1 at enzymatic activity level. *a*, GPX activity assay by spectrophotometry. Cell extract samples (700 μg/100 μl) were assayed spectrophotometrically for GPX activity as described in the text. One unit of GPX activity is defined as the amount of protein required to oxidize 1 μM NADPH per min. Values are means ± SD; $n = 3$. *, statistically significant difference in the activity when compared to SOD2; $P < 0.05$. Increased enzymatic activity was found in GPX1 transfectants. *b*, native activity gel assay for GPX activity. *Lane 1*, SOD2; *Lane 2*, Zeo35; *Lane 3*, S-GPX70; *Lane 4*, S-GPX86; *Lane 5*, S-GPX146; *Lane 6*, S-GPX182; *Lane 7*, S-GPX220. A total amount of 700 μg of protein from each cell clone was separated on an 8% native polyacrylamide gel with a 5% stacking gel. After electrophoresis, the gel was stained for GPX activity as described in the text. The achromatic band corresponding to GPX activity appeared on a blue background. GPX1 transfectants showed the brightest bands.

results (Fig. 2*b*) showed the expected new band (~ 1.8 kb) from the GPX1 transfectants as well as a band from the known endogenous GPX1 mRNA (~1 kb). The new band is exogenous GPX mRNA, the size of which corresponded to that of the *GPX* cDNA 1-kb fragment plus part of the sequence from the vector. We also demonstrated *GPX1* gene overexpression at the mRNA level using the RT-PCR method (Fig. 2*c*). Brighter bands were formed in the GPX1 transfectants, indicating that the mRNA levels of GPX1 were higher in the GPX transfectants than those in the control groups.

To examine whether the increased GPX1 protein was active, we measured the enzyme activity by spectrophotometric assay (Fig. 3*a*) and native gel electrophoresis analysis (Fig. 3*b*). The GPX1 activities of five clones (S-GPX70, S-GPX86, S-GPX146, S-GPX182, and S-GPX220) were 62.6 ± 6.0, 65.7 ± 4.5, 55.7 ± 3.5, 30.7 ± 2.8, and 45.9 ± 2.2 milliunits/mg of protein, respectively. The five clones have significant increases in GPX activity compared with both SOD2 (18.7 ± 1.2 milliunits/mg of protein) and Zeo35 (22.0 ± 5.0 milliunits/mg of protein). The results from native activity gels showed that the brightness of an activity gel band corresponds to the GPX1 activity of that clone (Fig. 3*b*). All GPX1 transfectants had much brighter bands than the control groups, SOD2 and Zeo35. The native gel result correlated with that of enzymatic activity assay. All activity results agreed with those found by Northern and Western blotting. We also ran a native activity gel assay for GR because its activity could be affected by GPX1 transfection; we saw little difference in GR activity among the different cell lines (data not shown).

Localization of GPX1 in the GPX1 Transfectants. The distribution of GPX1 protein in the GPX1 transfectants was determined by immunogold staining (Fig. 4). The immunogold staining indicated that GPX1 distributes not only to the cytoplasm (data not shown) but also to the mitochondria and the nucleus, which agrees with our previous results in adult hamster kidney (37). Thus, GPX1 was found in all three locations in the control cells, and the levels were increased in all three locations in the GPX1-overexpressing cells. Increases in the mitochondria and nucleus were unexpected because targeting sequences for these locations have not been noted.

GPX1 Modulates Changes in GSH and GSSG. In this part of our study, we seeded cells at 1×10^6 cells/100-mm dish and then harvested cells at 24 and 48 h after subculture. The total glutathione, GSH, and GSSG were measured as described in "Materials and Methods." The results from the samples harvested at 24 h after subculture are shown in Fig. 5*a*. There was a significant increase in the amount of total glutathione in Neo, S-GPX86, and S-GPX146 cells compared with the SOD2 clone. The amount of GSH increased in Neo and S-GPX146 cells compared with the SOD2 clone. GSSG significantly increased in S-GPX86 and S-GPX146 cells compared with the SOD2 clone, but GSSG dramatically decreased in P and S-GPX70 cells compared with SOD2 cells.

We also measured the total glutathione, GSH, and GSSG levels at 48 h after subculture. The results are shown in Fig. 5*c*. There were similar trends as the samples harvested at 24 h after subculture in the changes of total glutathione, GSH, and GSSG. The GSSG levels were significantly increased in all clones compared with their corresponding clones at 24 h except in S-GPX70.

Correlation analysis was performed on many of the data from this study. We first performed this analysis using the measured GPX activity values. We found poor correlations because P, Neo, and S-GPX70 were outliers. When we removed these cell lines, good correlations were obtained. The removal of P and Neo can easily be rationalized because they have a different genetic background; in particular, P and Neo have lower MnSOD levels than the other cell lines, which were all derived from the same MnSOD-overexpressing cell line (see Fig. 8). However, S-GPX70 has the same genetic background as other lines. In examining the data, we noticed that this line had much lower GSH levels than the others; thus, we hypothesized that S-GPX 70 was different from other GPX overexpressors because it did not have enough GSH for the GPX to maximally function. Because the rate of peroxide removal should be directly proportional to concentrations of both GPX and GSH, we thought that S-GPX70 data could be more congruent with other clones if we considered measured GPX activity times intracellular GSH as the dependent variable in all correlations. We call this the effective GPX activity and found the that the biological variables measured correlated very well with effective GPX. Thus, if correlation analysis was carried out with measured GPX activity as the dependent variable, much poorer correlations resulted than when effective GPX activity was used. We think that this reflects the actual biological situation in which the activity of GPX is limited by the levels of GSH. Because at normal physiological concentrations of GSH, GPX cannot saturated by GSH, this definition of effective GPX activity should be valid at all physiological concentrations of GSH (24)

Thus, in Fig. 5, *b* and *d*, we plotted GSSG *versus* effective GPX activity and found a good correlation. The GSH levels did not give a significant correlation (data not shown). Both [GSH]/[GSSG] and $[GSH]^2/[GSSG]$ have been used to indicate the redox state of the cell. Neither ratio gave us statistically significant correlations (data not shown). This could be because other factors, such as glucose utilization and $NADP^+$/NADPH ratios, need to be considered when measuring a redox balance.

The Changes in ROS Levels. The intracellular ROS levels were measured by the DCFH fluorescence method (Fig. 6*a*). This assay

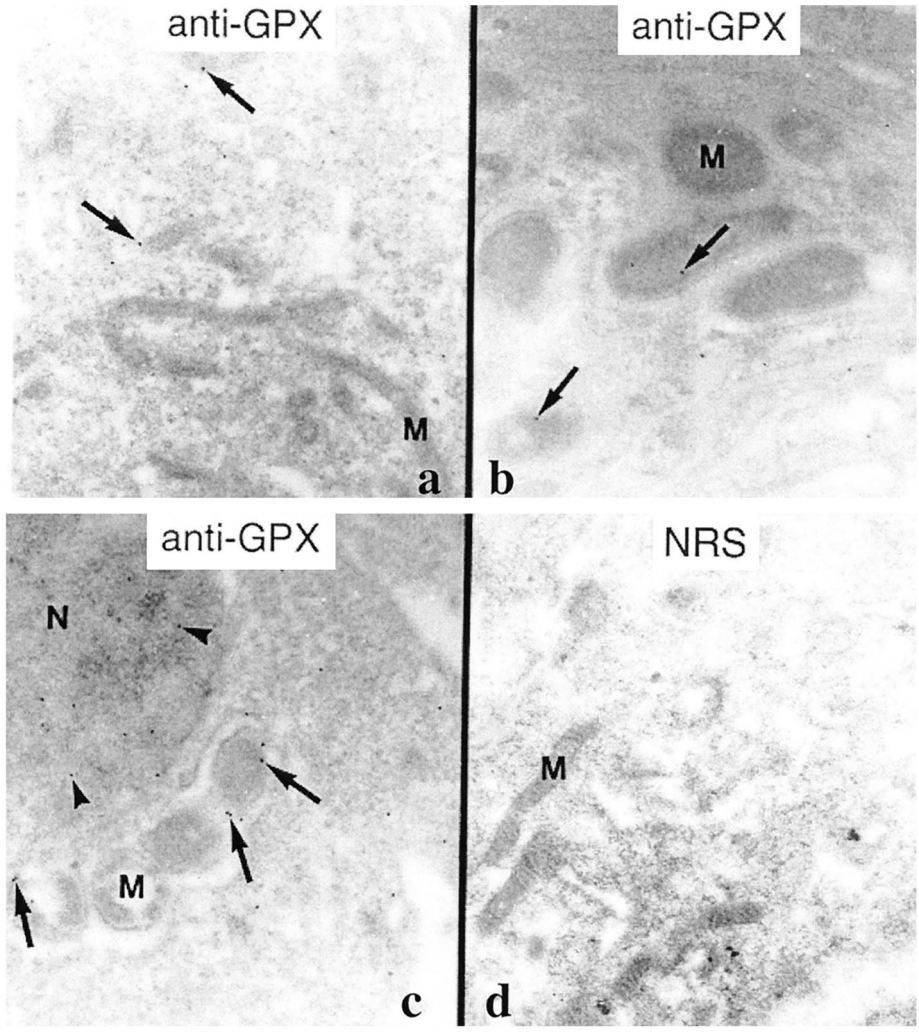

Fig. 4. Immunogold ultrastructural analysis of GPX1 immunoreactive protein localization. *a*, SOD2 cells treated with anti-GPX1 antibody. × 23100. *b*, Zeo35 cells treated with anti-GPX1 antibody. × 22300. *c*, S-GPX146 cells treated with anti-GPX1 antibody. × 23200. *d*, Zeo35 cells treated with normal rabbit serum (*NRS*) in place of primary antibody. × 23800. *M*, mitochondria; *N*, nucleus. *Arrows*, representative gold beads in mitochondria. *Arrowheads*, representative gold beads in nucleus.

measures oxidation by various ROS, including those derived from hydrogen peroxide. The intracellular ROS levels in SOD2 were dramatically increased to about 5-fold greater than P and 3-fold greater than Neo. The levels of intracellular ROS in the GPX transfectants, S-GPX86 and S-GPX146, were decreased about 3-fold and 2.5-fold, respectively, compared with SOD2, but there was no significant difference between S-GPX70 and SOD2. The levels of intracellular ROS were correlated to the levels of GPX1 and SOD activities. When DCFH fluorescence was plotted against effective GPX activity (Fig. 6*b*), a significant negative correlation was found ($r = -0.9192$; $P = 0.0273$).

GPX1 Inhibits IκB$_\alpha$ Degradation. To further study the effect of GPX1 on the intracellular redox status, we investigated the changes of IκB$_\alpha$ in the different clones by Western blotting assay (Fig. 7). IκB$_\alpha$ degradation is known to be activated by H_2O_2. There was a decrease in the level of IκB$_\alpha$ in SOD2 compared with both P and Neo and an increase in the level of IκB$_\alpha$ in all GPX-overexpressing clones compared with SOD2. S-GPX70 cells, which had increased GPX but also with a high level of intracellular ROS, also had high level of IκB$_\alpha$. Densitometry was performed on this Western blot; all of the GPX1-overexpressing clones had increased amounts of IκB$_\alpha$ immunoreactive protein when compared to the SOD2 cell line (Fig. 7). However, correlation analysis did not show a statistically significant correlation between the intensity of the Western bands and effective GPX activity (data not shown).

Western Blotting Assay for MnSOD, CuZnSOD, and CAT. We also determined whether there were any changes in the immunoreactive protein levels of MnSOD, CuZnSOD, and CAT by a Western blotting assay and densitometric analysis (Fig. 8). As expected, because they were derived from a MnSOD-overexpressing line, GPX1 transfectants and Zeo35 cells still kept the higher level of MnSOD overexpression compared with P cells and Neo cells. The level of MnSOD immunoreactive protein declined a small amount in GPX1 transfectants with passaging, but it was still higher than P and Neo cells (data not shown). The CuZnSOD level was slightly higher in Zeo35 cells and GPX1 transfectants than that in P, Neo, and SOD2 cells except for S-GPX86, which had very similar CuZnSOD levels to the SOD2 cells. For CAT, there was no great difference among the GPX1 transfectant groups and control groups except for Neo cells, which had a lower level of CAT protein, and S-GPX146, which had a slightly higher level of CAT protein. As mentioned earlier, the GPX overexpressors also showed little changes in GR activity. These data show that GPX1 overexpression does not cause great changes in other antioxidant proteins.

The Effect of GPX1 Overexpression on Tumor Cell Growth *in Vitro*. Tumor cell growth can be suppressed by MnSOD overexpression. We hypothesized that overexpression of MnSOD in human glioma cells results in an accumulation of H_2O_2 or other hydroperoxides, causing a decrease in glioma cell growth. We also hypothesized that transfection of these cells with the *GPX1* gene will rescue

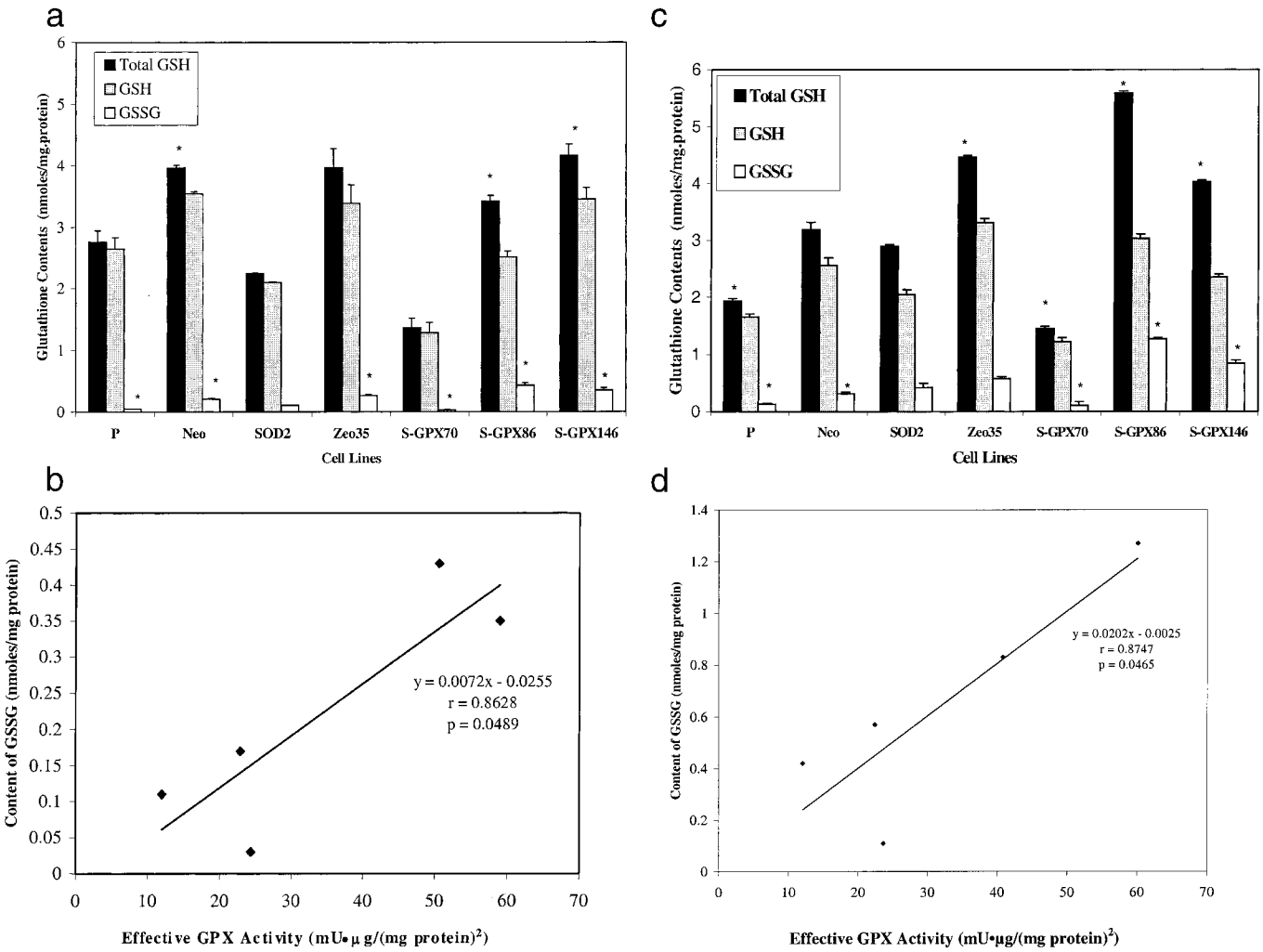

Fig. 5. Determination of intracellular redox state by measurement of total glutathione, GSH, and GSSG. *a*, assays of total glutathione, GSH, and GSSG in cells harvested at 24 h after subculture. Values are means ± SD; $n = 3$. *, $P < 0.05$ when compared with SOD2. *b*, correlation analysis of GSSG *versus* effective GPX activity. Cells were harvested at 24 h after subculture. *c*, assays of total glutathione, GSH, and GSSG in cells harvested at 48 h after subculture. Values are means ± SD; $n = 3$. *, $P < 0.05$ when compared with SOD2. *d*, correlation analysis of GSSG *versus* effective GPX activity. Cells were harvested at 48 h after subculture.

the growth inhibition of these cells through detoxification of H_2O_2 and/or changes in cellular redox status. To test these hypotheses, we measured cell growth rate *in vitro* by a growth curve (Fig. 9*a*), cell population doubling time (Fig. 9, *b* and *c*), and plating efficiency (Fig. 10, *a* and *b*).

Growth curves were performed by seeding cells in 24-well tissue culture plates at 2×10^4 per well and then counting cell number every other day. Fig. 9*a* shows that SOD2 and Zeo35 have the lowest growth rates, P and S-GPX70 have medium growth rates, and the other three clones (Neo, S-GPX86, and S-GPX146) have the highest growth rates. Neo also had a higher growth rate compared with P. One possible explanation for the difference in growth between P and Neo is the slight elevation of intracellular ROS concentration in Neo cells as shown in Fig. 6. In a broad sense, P is probably different from Neo because Neo was derived from P by selection and cloning. Somewhere in this process, a cell line with different properties arose. Cell population doubling times were calculated from cell growth curves (Fig. 9*b*). The cell population doubling times were 46.0 (P), 41.4 (Neo), 54.8 (SOD2), 52.4 (Zeo35), 48.6 (S-GPX70), 42.9 (S-GPX86), and 41.6 h (S-GPX146). As shown previously (5), SOD2 showed significant increases in the cell population doubling time compared with P and Neo. There were significant decreases in the cell population doubling times in S-GPX86 and S-GPX146 cells compared with SOD2. S-GPX70 also had a lower doubling time than SOD2, but the difference was not statistically significant. However, when correlation analysis was run on population doubling times *versus* effective GPX activity, a highly significant negative correlation was found (Fig. 9*c*; $r = -0.9747$; $P = 0.0048$). Population doubling time also showed highly significant correlation with DFCH fluorescence (Fig. 9*d*; $r = 0.7819$; $P = 0.0378$).

Plating efficiency is a measure of clonigenic ability of cells. For this assay, 500 cells were seeded in a 60-mm culture dish, and colonies were allowed to form for 2 weeks (Fig. 10*a*). The plating efficiency significantly decreased in the SOD2 line compared with P and Neo cells. There were significant increases in plating efficiency in S-GPX86 and S-GPX146 compared with SOD2. The plating efficiency of S-GPX70 was higher than that of SOD2, but the difference was not statistically significant. There was also no significant difference in colony formation ability between SOD2 and Zeo35. In general, the GPX1 transfection groups had higher ability to form colonies than SOD2 and Zeo35. Moreover, when plating efficiency was plotted against effective GPX activity (Fig. 10*b*) and correlation analysis was performed, a highly significant positive correlation was again found ($r = 0.9384$; $P = 0.0182$).

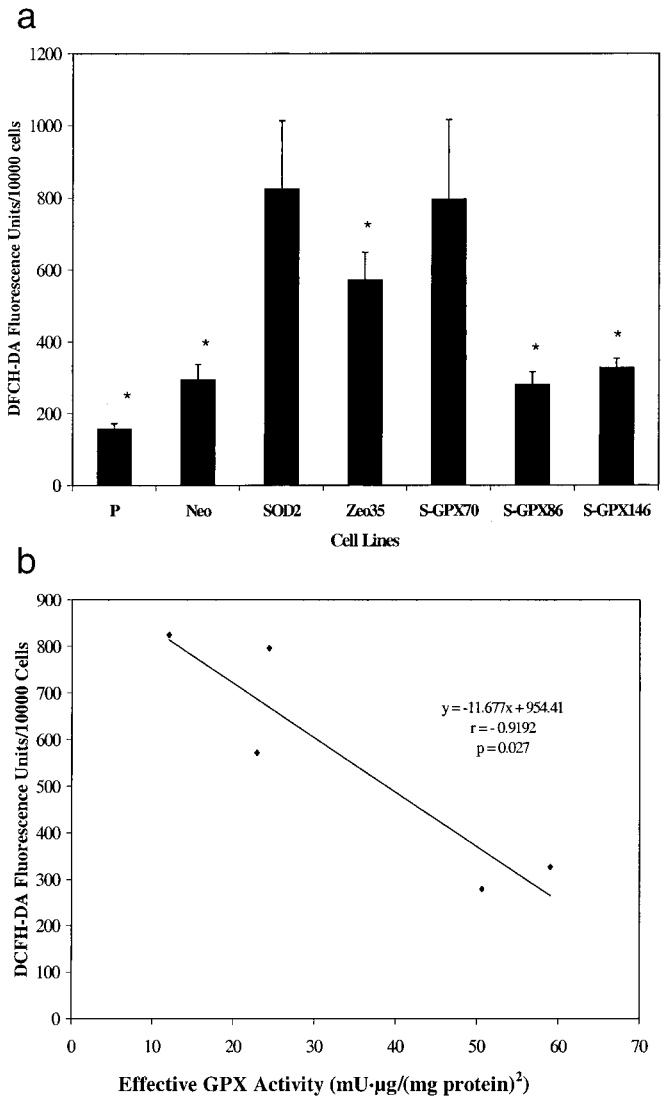

Fig. 6. Analysis of intracellular ROS. *a*, measurement of intracellular ROS in different samples. Cells were stained with DCFH-DA. The intensity of the 485/530 nm fluorescence of DCFH-DA, corresponding to the levels of intracellular ROS in the lysates were recorded with a microplate reader (Bio-Tek Instruments, Inc.) using FL500 software. *, $P < 0.05$ when compared with SOD2. In general, cells with high GPX activity had lowered levels of DCFH fluorescence. *b*, correlation analysis of intracellular ROS *versus* effective GPX activity.

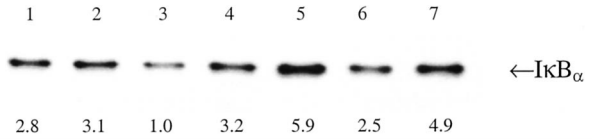

Fig. 7. Analysis of $I\kappa B_\alpha$ in different clones. One hundred μg of total protein from each clone were separated in a 12.5% SDS-PAGE gel and electrotransferred onto a nitrocellulose membrane. The blots were probed with primary $I\kappa B_\alpha$ antibody and then a horseradish peroxidase conjugated with goat antirabbit IgG. The bands corresponding to $I\kappa B_\alpha$ were detected by the ECL method. *Lane 1*, P; *Lane 2*, Neo; *Lane 3*, SOD2; *Lane 4*, Zeo35; *Lane 5*, S-GPX70; *Lane 6*, S-GPX86; *Lane 7*, S-GPX146. Results from densitometric analysis are shown *under* each lane; the fold increase relative to cell line SOD2 is given. In general, cells with high GPX activity had increased levels of $I\kappa B_\alpha$ immunoreactive protein.

The Effect of GPX1 Overexpression on Tumor Cell Growth *in Vivo*. Tumorigenicity was determined by transplanting tumor cells in the back of the neck of nude mice. This experiment was designed to test the role of GPX1 redox regulation in the suppression of tumor cell growth by MnSOD *in vivo*. The results of the tumor growth experiment are shown in Fig. 11*a* and Table 1. The MnSOD-overexpressing cell line formed tumors that grew much slower than the P or Neo cell line. S-GPX86 and S-GPX146 had the highest growth rates (Fig. 11*a*). All of the GPX-overexpressing cell lines grew faster than the SOD2 line from which they were derived. When the tumor volume at day 63 was plotted against effective GPX activity and correlation analysis was performed, a highly significant positive correlation was found ($r = 0.9899$; $P = 0.002$; Fig. 11*b*). These results show convincingly that GPX overexpression inhibits the growth suppression caused by MnSOD overexpression. Tumor incidence showed a similar picture (Table 1). P and Neo had a high tumor incidence, which was suppressed by MnSOD overexpression. GPX and MnSOD double overexpressors again had a high tumor incidence, showing that GPX can inhibit the tumor suppressive ability of MnSOD.

DISCUSSION

MnSOD has been proposed to be a new type of tumor suppressor gene (38). Most types of tumor cells have reduced levels of this protein when compared with their normal cell counterparts. Numerous studies have demonstrated that transfection of *MnSOD* cDNA into various tumor cells results in decreasing their tumorigenicity. Transfection of the human *MnSOD* cDNA into MCF-7 breast cancer cells (2), UACC-903 melanoma cells (3), SCC-25 oral squamous carcinoma cells (4), U118 human glioma cells (5), and DUI45 human prostate carcinoma cells (6) significantly suppressed their malignant phenotype, leading to lower clonogenicity and growth suppression in nude mice. Adenovirus-mediated *MnSOD* gene transfer to hamster cheek pouch carcinoma cells caused effective growth suppression *in vitro* (7). Zhong *et al.* (39) reported that overexpression of MnSOD in rat glioma cells not only inhibited cell growth but also resulted in sensitization to oxidative damage. Taken together, these studies provide *in vitro* and *in vivo* evidence of tumor suppressor effects of MnSOD, but the mechanism(s) by which this antioxidant enzyme suppresses the malignant phenotype is currently unclear.

GPX1 belongs to the family of selenoproteins and plays an important role in the defense mechanisms of mammals against damage by

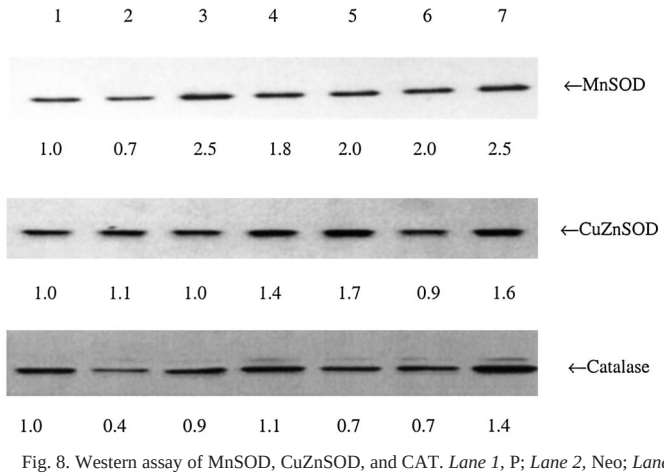

Fig. 8. Western assay of MnSOD, CuZnSOD, and CAT. *Lane 1*, P; *Lane 2*, Neo; *Lane 3*, SOD2; *Lane 4*, Zeo35; *Lane 5*, S-GPX70; *Lane 6*, S-GPX86; *Lane 7*, S-GPX146. Total proteins (10 μg for MnSOD, 50 μg for CuZnSOD and CAT) from each clone were separated in a 12.5% SDS-PAGE gel and electrotransferred onto a nitrocellulose membrane. The blots were probed with primary MnSOD antibody, CuZnSOD antibody, and CAT antibody, respectively, and then with a horseradish peroxidase conjugated with goat antirabbit IgG. The bands corresponding to MnSOD, CuZnSOD, and CAT were detected by the ECL method. Results from densitometric analysis are shown *under* each lane; the fold increase relative to the P cell line is given. MnSOD immunoreactive protein was high in all clones derived from SOD2, but no large or consistent changes were observed in CuZnSOD or CAT immunoreactive protein.

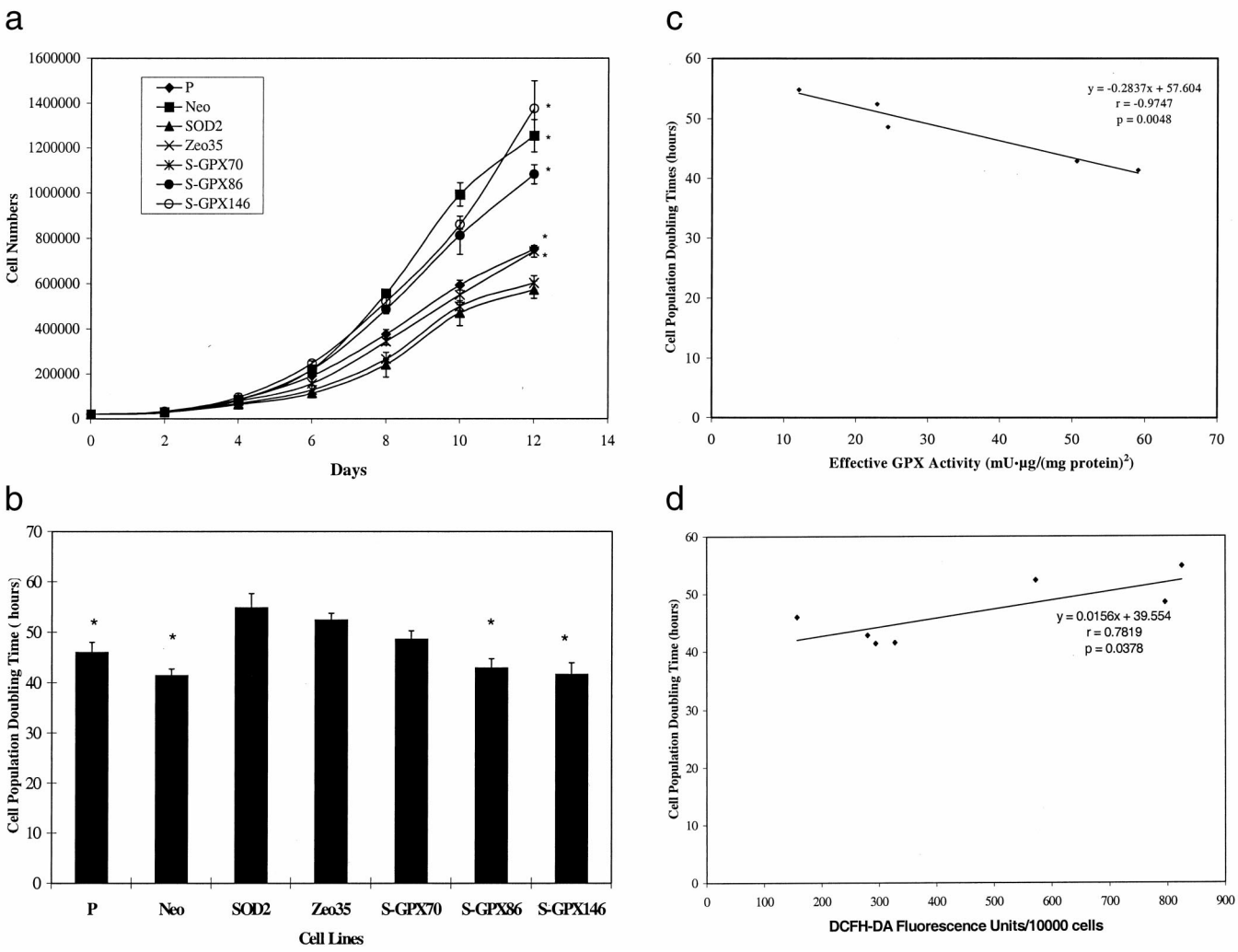

Fig. 9. Effect of GPX1 overexpression on cell growth *in vitro*. *a*, growth curve. Twenty thousand cells were seeded in 24-well plates. Cell number was counted on days 2, 4, 6, 8, 10, and 12. Values are means ± SD; $n = 3$. *, $P < 0.05$ when compared with SOD2 at day 12. The results show that SOD2 inhibited tumor cell growth, whereas overexpression of GPX1 alleviated this growth suppression. *b*, cell population doubling time (T_d). Cell population doubling time was calculated from cell growth curve according to the equation $T_d = 0.693/\ln(N_t/N_0)$, where t is time in hours, N_t is the cell number at time t, and N_0 is the cell number at initial time. Values are means ± SD; $n = 3$. *, $P < 0.05$ when compared with SOD2. Again, the SOD2 cell line had the highest doubling time, and GPX1 overexpression led to decreased doubling times. *c*, correlation analysis of doubling times *versus* effective GPX activity. *d*, correlation analysis of cell population doubling time *versus* intracellular ROS levels.

catalyzing the reduction of H_2O_2 and a large variety of hydroperoxides (such as DNA hydroperoxides and lipid hydroperoxides) into water and alcohols, respectively, with GSH as the hydrogen donor (40). GPX1 is usually thought of as a cytosolic protein. We have shown previously that GPX1 is also found in the nucleus and mitochondria (37). In the present study all these subcellular compartments stained more intensely after GPX1 overexpression; this shows the specificity of our antibody as well as multiple subcellular localizations. Utsunomiya *et al.* (41) and Asayama *et al.* (42) have shown immunohistostaining of mitochondria, nuclei, and cytosol with polyclonal antirat GPX1 antiserum, which also suggested that GPX1 has multiple subcellular localizations. Using *GPX1* knockout mice, Esworthy *et al.* (43) provided direct evidence suggesting that the *GPX1* gene encodes mitochondrial GPX in mouse liver. Taken together, it is most likely that the GPX1 has mitochondrial, nuclear, and cytosolic subcellular locations in mammalian cells. Unlike phospholipid hydroperoxide GPX, there in no presequence that mediates GPX1 translocation into mitochondria. Therefore, the mechanism whereby GPX1 is imported into mitochondria is unclear. The same is true for import into the nucleus.

Aerobic organisms generate toxic ROS during oxidative metabolism or under pathological conditions. Organisms have evolved antioxidant defenses to protect against ROS, predominant among which is the enzymatic antioxidant pathway (Fig. 1). This pathway suggests that overexpression of SOD without concomitant increase in the level of GPX1 results in the accumulation of H_2O_2 that not only changes the cellular redox status but also can participate in the Fenton reaction, leading to production of noxious hydroxyl radicals. In this study, we hypothesized that overexpression of MnSOD in human glioma cells results in an accumulation of H_2O_2 or other hydroperoxides causing a decrease in glioma cell growth. We further hypothesized that transfection of these cells with the human *GPX1* gene will rescue the growth of these cells through detoxification of H_2O_2 and/or changes in cellular redox status.

The findings here indicate that overexpression of GPX1 rescues the growth suppression by MnSOD (Fig. 9*a*). The growth characteristics of different clones correlated to their intracellular ROS levels (Fig. 9*d;* $r = 0.7819$; $P = 0.0378$). SOD2 cells with the highest ROS levels had the lowest growth rate, longest doubling time (Fig. 9*b*), and lowest plating efficiency (Fig. 10*a*), whereas GPX1 transfectants (S-GPX86. S-GPX146) and Neo cells with lower levels of ROS had the highest growth rates, shortest doubling times, and highest plating efficiencies.

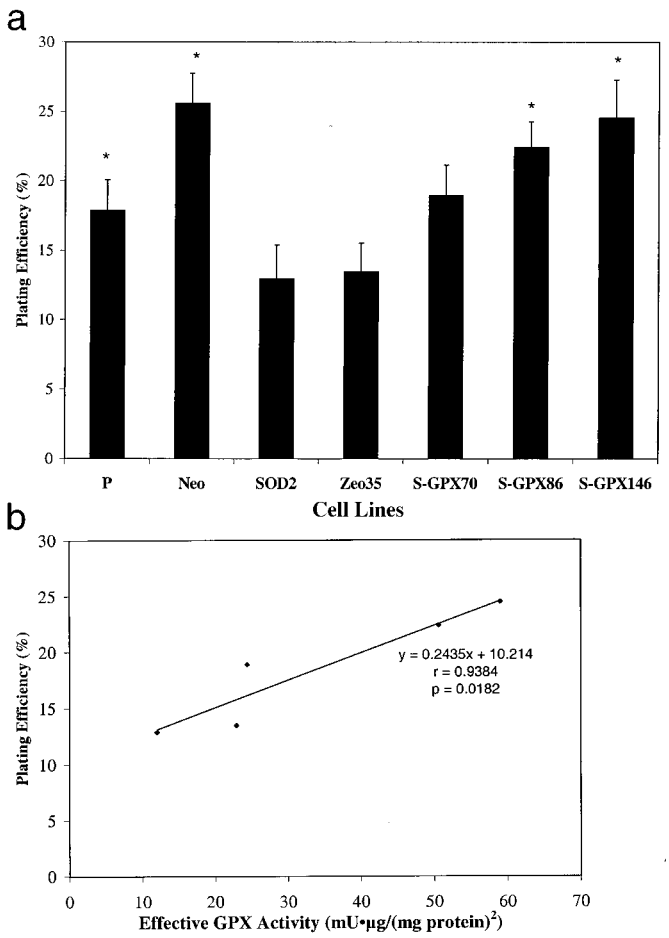

Fig. 10. Effect of GPX1 overexpression on cell plating efficiency. *a*, cell plating efficiency. Five hundred cells were seeded in 60-mm dishes and grown for 2 weeks. Colonies with more than 50 cells were counted. Values are means ± SD; $n = 3$. *, $P < 0.05$ when compared with SOD2. The SOD2 cell line had low plating efficiency that was elevated by GPX1 overexpression. *b*, correlation analysis of plating efficiency *versus* effective GPX activity.

Similar results were found *in vivo* in nude mice studies; MnSOD overexpression inhibited tumor cell growth and lowered tumor incidence; GPX1 overexpression inhibited such tumor suppression. SODs convert $O_2^{\cdot-}$ into H_2O_2, whereas GPX1 and CAT convert H_2O_2 into water. In this way, two toxic species, $O_2^{\cdot-}$ and H_2O_2, are converted into the harmless product water. Higher activities of GPX1 resulted in decreased levels of ROS in the S-GPX86 and S-GPX146 cells. S-GPX70 also had high GPX1 activity, but these cells could not remove H_2O_2 efficiently as shown by high DCFH fluorescence. This may result from the fact that there was not enough GSH in the S-GPX70 cells (Fig. 5, *a* and *c*). The removal of H_2O_2 by GPX1 requires GSH as cofactor. These results indicate that GPX1 overexpression can dramatically abolish the growth suppression by MnSOD overexpression when there is enough GSH in cells and suggest that H_2O_2 or other hydroperoxides are involved in such growth suppression. The observation that S-GPX70 line did not behave as the other GPX-overexpressing lines let us to formulate the effective GPX activity concept: effective GPX activity equals measured GPX activity times intracellular GSH concentration. This concept is based on the simple principle that the rate of an enzymatic reaction is proportional to the substrate concentration until the enzyme becomes saturated; because GPX does not become saturated with GSH under normal physiological conditions, in cells the reaction rate will generally be proportional to GSH levels (24). When we used effective GPX activity, S-GPX70 was no longer an outlier in any of our measurements. These results suggest that effective GPX activity should be used to quantify the actual peroxide removed by this system. Our results suggest that effective GPX activity is what governed the biological response of all GPX-overexpressing cell lines, although we cannot rule out the possibility that the small changes in MnSOD observed in these lines had some effect on the observed phenotype.

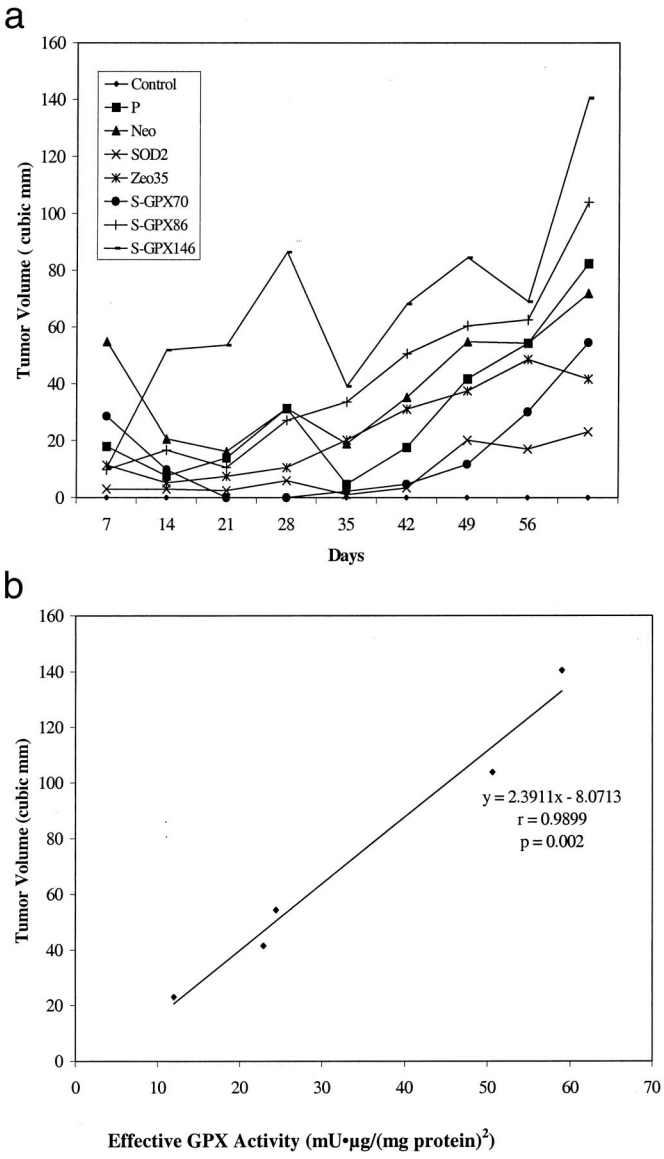

Fig. 11. Effect of GPX1 overexpression on tumor growth *in vivo*. Tumorigenicity in female nude mice. Two million cells were transplanted in the back of the neck of female nude mice. Tumor length (*L*) and width (*W*) were measured once a week by vernier caliper. Tumor volume (*TV*) was calculated by the formula $TV = L \times W^2/2$. There were four mice in each group and all mice were included in calculations of tumor volume. *a*, tumor growth curve *in vivo*. *b*, correlation analysis of tumor volume at day 63 *versus* effective GPX activity. The results show that MnSOD overexpression inhibits tumor cell growth and GPX overexpression inhibits such tumor suppression.

Table 1 *Tumor incidence*[a]

	Cell line						
	P	Neo	SOD2	Zeo35	S-GPX70	S-GPX86	S-GPX146
Incidence (%)	57.1 (4/7)	62.5 (5/8)	25 (2/8)	37.5 (3/8)	25 (2/8)	75 (6/8)	85.7 (6/7)

[a] Tumor incidence = (number of mice with tumor/total number of total mice) × 100. The data are from two experiments, usually with four mice per group in each experiment.

In mammalian cells, overexpression of SOD in cells bearing extra copies of the SOD gene produced a higher sensitivity to ROS. In these cases, it has been postulated that SOD overexpression would lead to accumulation of H_2O_2 (15, 44). In addition, overexpression of CuZnSOD can cause different responses in different systems. A compensatory increase in GPX1 occurred as a consequence of the introduction of the CuZnSOD expression vector into L-cells, neuroblastoma cells and primary mouse cells (45, 46). Transfection of human glioma cells with human *MnSOD* can also induce a GPX1 activity increase (5). Transfection of a *CuZnSOD* expression vector into 3T3 murine fibroblasts resulted in two classes of transfectants, characterized by the presence or absence of an increase in endogenous GPX1. In the transfectants with an absence of an increase in endogenous GPX1, accumulation of H_2O_2 was increased (47). Fullerton *et al.* (48) found that transgenic brain accumulated H_2O_2 after perinatal hypoxia ischemia in CuZnSOD transgenic mice. In JB6 cells and Chinese hamster fibroblasts, overexpression of CuZnSOD resulted in increased DNA breakage upon exposure to oxidants (15, 16). Amstad *et al.* (15) studied the roles of and the interaction of CuZnSOD and CAT in transfectants with human cDNAs of mouse epidermal JB6 clone 41 cells. The CuZnSOD overproducers SOD 15 and SOD 3 were hypersensitive to the formation of DNA single strand breaks, growth retardation, and killing by an extracellular burst of O_2^- plus H_2O_2, whereas CAT overproducers were protected from oxidant damage relative to the parent clone JB6 clone 41. The double transfectant SOCAT 3 was better protected from oxidant damage because of its increased content of CAT, which counterbalances the increase in CuZnSOD. In 1994, Amstad *et al.* (17) reported that GPX1 also compensated for the hypersensitivity of CuZnSOD overproducers to oxidant stress. Taken together, our results and those of others clearly indicate that after overexpression of SOD, H_2O_2 appears to be a key player in the growth of SOD transfectants; the balance of SOD and GPX or CAT is more important for overall sensitivity than the level of SOD alone, and growth stimulation occurs when cells are protected from excessive oxidative stress.

In the growth rate results, we also found that Neo cells grew faster than P cells. This might result from the fact that Neo cells had higher intracellular ROS levels than P cells and suggests that intracellular ROS can stimulate cell growth at certain levels. A number of normal cells and tumors can produce H_2O_2 and O_2^- *in vitro* either in response to various stimulus or constitutively (15). Experiments in which either CAT or SOD was added exogenously to the growth medium of hamster, rat fibroblasts (49), and HeLa cells (50) resulted in a depressed rate of cell proliferation. Other experiments (51, 52) also indicated low concentrations of O_2^- and H_2O_2 (10 nM-1 μM) to be effective in stimulating the *in vitro* growth of hamster and rat fibroblasts when added to the culture medium. Using xanthine/xanthine oxidase (100 μM xanthine and 5 microunits/ml xanthine oxidase) to generate ROS, Rao and Berk (53) demonstrated that H_2O_2 can stimulate rat vascular smooth muscle cell growth. This evidence suggests that H_2O_2 and O_2^- can stimulate growth and growth responses in a variety of cultured mammalian cell types when produced endogenously or added exogenously.

GPX1 converts H_2O_2 to H_2O and catalyzes GSH to GSSG simultaneously. Our results show that overexpression of GPX1 modulated the content of intracellular GSH and GSSG (Fig. 5). The amount of GSSG in S-GPX70 cells was the lowest among all of the clones. This result was not correlated to the measured GPX activity of S-GPX70. As discussed earlier, this result may be from lower amount of GSH in S-GPX70 compared with other transfectants. Because GPX requires GSH as a cofactor to exert its function, the lower GSH will limit the maximum activity of GPX. When GSSG was plotted against effective GPX activity, good correlation resulted (Fig. 5, *b* and *d*), and S-GPX70 was no longer an outlier.

We also found evidence to suggest that metabolism also affected the content of glutathione. The content of GSSG significantly increased in all clones except S-GPX70, whereas the ratio (data not shown) between $[GSH]^2/[GSSG]$ was dramatically decreased in all clones at 48 h compared with those at 24 h. Because glucose will be probably depleted during this time period, these results suggest that glucose can influence the levels of intracellular glutathione. We hypothesize that the concentration of glucose is becoming lower with time after feeding. The lower concentration of glucose leads the cells to produce less NADPH through the pentose phosphate pathway. This does not enable GR to fully function without enough NADPH, which causes the accumulation of GSSG. Blackburn *et al.* (54) recently demonstrated that glucose deprivation significantly increased the steady state levels of GSSG.

GSH and GSSG are important components in the cellular redox system. The GSH/GSSG couple is the major redox buffer in the cell (23, 24). GSH is a tripeptide of γ-glutamate, cysteine, and glycine, which is found ubiquitously in eukaryotic cells at a concentration between 1 and 10 mM (24). The relationship among intracellular GSH, GSSG, and GSH/GSSG or $[GSH]^2/[GSSG]$ ratio is more complicated. They are governed by the rate of synthesis of GSH, the prevailing oxidative state, the activities of GPX and GR, the degree of export of GSH and GSSG from the cell, and compartmentalization of these molecules. Most cell types do not import GSH (55), and synthesis occurs intracellularly in sequential, ATP-dependent reactions catalyzed by γ-glutamylcysteine synthetase and GSH synthetase. The rate of synthesis is influenced primarily by the availability of cysteine but also by feedback inhibition of synthesis by GSH. Conversion of GSH to GSSG occurs during GPX1-catalyzed reduction of H_2O_2 and other peroxides and in spontaneous reactions with free radicals (56). GSSG is restored to a reduced form by GR (57). Irreversible loss of GSH occurs through conjugation to endogenous and exogenous electrophilic centers in reactions catalyzed by GSH transferases (58, 59).

The intracellular ROS levels as measured by DCFH-DA fluorescence were also modulated by GPX1 overexpression (Fig. 6). The results of intracellular ROS levels suggest that MnSOD overexpression leads to accumulation of H_2O_2, which causes high fluorescence intensity of DCFH-DA. GPX1 can remove H_2O_2, so there was low fluorescence intensity in both S-GPX86 and S-GPX146 clones. Although S-GPX70 has high GPX activity, there was no significant difference between SOD2 and S-GPX70 in ROS levels. This result implies that GPX1 in S-GPX70 cells cannot exert its full function because this clone has lower GSH content compared with the other clones. This result also implies that GSH is very important to make GPX function. Again, this conclusion was strengthened by a correlation analysis; a high correlation resulted when DCFH fluorescence was plotted against effective GPX activity (Fig. 6*b*).

Our results also indicated that overexpression of GPX1 inhibited $I\kappa B_\alpha$ degradation (Fig. 7). The levels of intracellular ROS as measured by DCFH fluorescence correlated well with the effective GPX activity (Fig. 6*b*); this, along with the Western blot of $I\kappa B_\alpha$ (Fig. 7), suggests that ROS can cause $I\kappa B_\alpha$ degradation and that GPX1 can inhibit this process. These results are consistent with the results reported by Kretz-Remy *et al.* (27). They demonstrated that $I\kappa B_\alpha$ degradation was abolished in GPX1-overexpressing T47D cells exposed to TNF-α and H_2O_2. There was also an exception to the general result shown in Fig. 6*a*. S-GPX70 cells with high levels of ROS also have high levels of $I\kappa B_\alpha$, which implies that other factors such as GSSG besides ROS can cause $I\kappa B_\alpha$ degradation. Droge *et al.* (60) have found that T cells fail to activate NF-κB in response to appropriate stimuli at low levels of cytosolic GSSG. Recently, Kroll *et al.*

(61) reported that inducible degradation of $I\kappa B_\alpha$ by the proteasomes requires interaction with the F-box protein h-βTrCP. Theoretically, GPX1 can regulate the cellular redox state by modulating the concentrations of the H_2O_2, GSH, GSSG, NADPH, and $NADP^+$ molecules that are critical players in the cellular redox system (Fig. 1). In HIV-infected T-cells (25) and in similar T-cell lines (26), selenium supplementation increased GPX activity and decreased H_2O_2-induced NF-κB activation. A human breast cancer cell line (T47D) overexpressing GPX1 responded poorly to NF-κB activation by TNF-α or H_2O_2; both κB-dependent gene transactivation and NF-κB DNA binding were reduced (27). Taken together, our findings and those of others demonstrate that GPX1 plays a key role in the regulation of cellular redox state.

In conclusion, our results show the following. First, GPX1 overexpression in MnSOD-overexpressing cells can rescue cell growth suppressed by MnSOD, which suggests that H_2O_2 or other hydroperoxides are critical reactants in the glioma tumor suppression by MnSOD overexpression. Second, GPX1 overexpression can modulate intracellular redox status and inhibit $I\kappa B_\alpha$ degradation. Third, GPX1 exists not only in cytosol but also in the mitochondria and nucleus. Our results also suggest that effective GPX activity should be used to quantify the actual peroxide removed by this system. Taken together, our data show that MnSOD overexpression inhibits tumor growth because of the production of hydroperoxides and suggest that inhibition of peroxide removal should increase the tumor suppressive effect of MnSOD overexpression.

ACKNOWLEDGMENTS

We thank Dr. James H. Doroshow for the gift of the human *GPX1* cDNA.

REFERENCES

1. Oberley, L. W., and Buettner, G. R. Role of superoxide dismutase in cancer: a review. Cancer Res., *39:* 1141–1149, 1979.
2. Li, J. J., Oberley, L. W., St. Clair, D. K., Ridnour, L. A., and Oberley, T. D. Phenotypic changes induced in human breast cancer cells by overexpression of manganese-containing superoxide dismutase. Oncogene, *10:* 1989–2000, 1995.
3. Church, S. L., Grant, J. W., Ridnour, L. A., Oberley, L. W., Swanson, P. E., Meltzer, P. S., and Trent, J. M. Increased manganese superoxide dismutase expression suppresses the malignant phenotype of human melanoma cells. Proc. Natl. Acad. Sci. USA, *90:* 3113–3117, 1993.
4. Liu, R., Oberley, T. D., and Oberley, L. W. Transfection and expression of MnSOD cDNA decreases tumor malignancy of human oral squamous carcinoma. Hum. Gene Ther., *8:* 585–595, 1997.
5. Zhong, W., Oberley, L. W., Oberley, T. D., and St. Clair, D. K. Suppression of the malignant phenotype of human glioma cells by overexpression of manganese superoxide dismutase. Oncogene, *14:* 481–490, 1997.
6. Li, N., Oberley, T. D., Oberley, L. W., and Zhong, W. Overexpression of manganese superoxide dismutase in DU145 human prostate carcinoma cells has multiple effects on cell phenotype. Prostate, *35:* 221–233, 1998.
7. Lam, E. W. N., Zwacka, R., Engelhardt, J. F., Davidson, B. L., Domann, F. E., Jr., Yan, T., and Oberley, L. W. Adenovirus-mediated manganese superoxide dismutase gene transfer to hamster cheek pouch carcinoma cells. Cancer Res., *57:* 5550–5556, 1997.
8. Mills, G. C. Glutathione peroxidase, an erythrocyte enzyme that protects hemoglobin from oxidative damage. J. Biol. Chem., *229:* 189–197, 1957.
9. Hann, J. B., Bladier, C., Griffiths, P., Kelner, M., O'Shea, R. D., Cheung, N. S., Bronson, R. T., Silvestro, M. J., Wild, S., Zheng, S. S., Beart, P. M., Hertzog., and Kola, I. Mice with homozygous null mutation for the most abundant glutathione peroxidase, GPX1, show increased susceptibility to the oxidative stress-inducing agents paraquat and hydrogen peroxide. J. Biol. Chem., *273:* 22528–22536, 1998.
10. Mirault, M-E., Tremblay, A., Beaudoin, N., and Tremblay, M. Overexpression of seleno-glutathione peroxidase by gene transfer enhances the resistance of T47D human breast cells to clastogenic oxidants. J. Biol. Chem., *266:* 20752–20760, 1991.
11. Kelner, M. J., Bagnell, R. D., Uglik, S. F., Montoya, M. A., and Mullenbach, G. T. Heterologous expression of selenium-dependent glutathione peroxidase afford cellular resistance to paraquat. Arch. Biochem. Biophys., *323:* 40–46, 1995.
12. Sies, H., Sharov, V. S., Klotz, L-O., and Briviba, K. Glutathione peroxidase protects against peroxynitrite-mediated oxidation. J. Biol. Chem., *272:* 27812–27817, 1997.
13. Hockenbery, D. M., Oltvai, Z. N., Yin, X., Milliman, C. L., and Korsmeyer, S. J. Bcl-2 functions in an antioxidant pathway to prevent apoptosis. Cell, *75:* 241–251, 1993.
14. Kayanoki, Y., Fujii, J., Islam, K. N., Suzuki, K., Kawata, S., Matsuzawa, Y., and Taniguchi, N. J. The protective role of glutathione peroxidase in apoptosis induced by reactive oxygen species. Biochemistry, *119:* 817–822, 1996.
15. Amstad, P., Peskin, A., Shah, G., Mirault, M. E., Moret, R., Zbinden, I., and Cerutti, P. The balance between Cu,Zn-superoxide dismutase and catalase affects the sensitivity of mouse epidermal cells to oxidative stress. Biochemistry, *30:* 9305–9313, 1991.
16. Teixeira, H. D., and Meneghini, R. Chinese hamster fibroblasts overexpressing CuZn-superoxide dismutase undergo a global reduction in antioxidants and increase sensitivity of DNA to oxidative damage. Biochem. J., *315:* 821–825, 1995.
17. Amstad, P., Moret, R., and Cerutti, P. Glutathione peroxidase compensates for the hypersensitivity of Cu,Zn-superoxide dismutase overproducers to oxidant stress. J. Biol. Chem., *269:* 1606–1609, 1994.
18. Burdon, R. H. Superoxide and hydrogen peroxide in relation to mammalian cell proliferation. Free Radical Biol. Med., *18:* 775–794, 1995.
19. Powis, G., Briehl, M., and Oblong, J. Redox signaling and the control of cell growth and death. Pharmacol. Ther., *68:* 149–173, 1995.
20. Sen, CK., and Packer, L. Antioxidant and regulation of gene transcription. FASEB J., *10:* 709–720, 1996.
21. Sun, Y., and Oberley, L. W. Redox regulation of transcriptional activators. Free Radical Biol. Med., *21:* 335–348, 1996.
22. Suzuki, Y. J., Forman, H. J., and Sevanian, A. Oxidants as stimulators of signal transduction. Free Radical Biol. Med., *22:* 269–285, 1997.
23. Meister, A., and Anderson, M. E. Glutathione. Annu. Rev. Biochem., *52:* 711–760, 1983.
24. Kosower, N. S., and Kosower, E. M. The glutathione status of cells. Int. Rev. Cytol., *54:* 109–160, 1978.
25. Sappey, C., Legrand-Poels, S., Best-Belpomme, M., Favier, A., Rentier, B., and Piette, J. Stimulation of glutathione peroxidase activity decreases HIV type activation after oxidative stress. AIDS Res. Hum. Retroviruses, *10:* 451–1461, 1994.
26. Makropoulos, V., Brening, T., Schulze-Osthoff, K. Selenium-mediated inhibition of transcription factor 78 F-κ-B and HIV-1 LTR promoter activity. Arch. Toxicol., *70:* 277–283, 1996.
27. Kretz-Remy, C., Mehlen, P., Mirault, M-E., and Arrigo, A-P. Inhibition of I-κ-B phosphorylation and degradation and subsequent NF-κ-B activation by glutathione peroxidase overexpression. J. Cell. Biol., *133:* 1083–1093, 1996.
28. Omar, B. A., and McCord, J. M. The cardioprotective effect of Mn-superoxide dismutase is lost at high doses in the postischemic isolated rabbit heart. Free Radical Biol. Med., *9:* 473–478, 1990.
29. Sun, Y., Oberley, L. W., Oberley, T. D., Elwell, J. H., and Sierra-Rivera, E. Lowered antioxidant enzymes in spontaneously transformed embryonic mouse liver cells in culture. Carcinogenesis, *14:* 1457–1463, 1993.
30. Sukenaga, Y., Ishida, K., Takeda, T., and Takagi, K. Nucleotide sequence of a human gene for glutathione peroxidase. Nucleic Acids Res., *15:* 17, 1987.
31. Lawrence, R. A., and Burk, R. F. Glutathione peroxidase activity in selenium-deficient rat liver. Biochem. Biophys. Res. Commun., *71:* 952–958, 1976.
32. Yan, T., Jiang, X., Zhang, H. J., Li, S., and Oberley, L. W. Use of commercial antibodies for detection of the primary antioxidant enzymes. Free Radical Biol. Med., *25:* 688–693, 1998.
33. St. Clair, D. K., Wan, X. S., Oberley, T. D., Muse, K. E., and St. Clair, W. H. Suppression of radiation-induced neoplastic transformation by overexpression of mitochondrial superoxide dismutase. Mol. Carcinog., *6:* 238–242, 1992.
34. Bullard, D. E., Schold, S. C., Bigner, S. H., and Bigner, D. D. Growth and therapeutic response in athymic mice of tumors arising from human glioma-derived cell lines. J. Neuropathol. Exp. Neurol., *40:* 410–427, 1981.
35. Anderson, M. E. Tissue glutathione. *In:* R. A. Greenwald (Ed.), Handbook of Methods for Oxygen Radical Research, pp. 317–323. Boca Raton, FL: CRC Press, 1985.
36. Royall, J. A., and Ischiropoulos, H. Evaluation of 2′,7′-dichlorofluorescin and dihydrorhodamine 123 as fluorescent probes for intracellular H_2O_2 in cultured endothelial cells. Arch. Biochem. Biophys., *302:* 348–355, 1993.
37. Muse, K. E., Oberley, T. D., Sempf, J. M., and Oberley, L. W. Immunolocalization of antioxidant enzymes in adult hamster kidney. Histochem. J., *26:* 734–753, 1994.
38. Bravard, A., Sabatier, L., Hoffschir, F., Ricoul, M., Luccioni, C., and Dutrillaux, B. SOD2: a new type of tumor-suppressor gene? Int. J. Cancer, *51:* 476–480, 1992.
39. Zhong, W., Oberley, L. W., Oberley, T. D., Yan, T., Domann, F. E., and St. Clair, D. K. Inhibition of cell growth and sensitization to oxidative damage by overexpression of manganese superoxide dismutase in rat glioma cells. Cell Growth Differ., *7:* 1175–1186, 1996.
40. Freeman, A. U., and Crapo, J. D. Biology of disease: free radicals and tissue injury. Lab. Invest., *47:* 412–426, 1982.
41. Utsunomiya, H., Komatsu, N., Yoshimura, S., Tsutsumi, Y., and Watanabe, K. Exact ultrastructural localization of glutathione peroxidase in normal rat hepatocytes: advantages of microwave fixation. J. Histochem. Cytochem., *39:* 1167–1174, 1991.
42. Asayama, K., Yokota, S., Dobashi, K., Hayashibe, H., Kawaoi, A., and Nakazawa, S. Purification and immunoelectron microscopic localization of cellular glutathione peroxidase in rat hepatocytes: quantitative analysis by postembedding method. Histochemistry, *102:* 213–219, 1994.
43. Esworthy, R. S., Ho, Y. S., and Chu, F. F. The *GPX1* gene encodes mitochondrial glutathione peroxidase in the mouse liver. Arch. Biochem. Biophys., *340:* 59–63, 1997.
44. Elroy-Stein, O., Bagnell, Y., and Groner, Y. Overproduction of human Cu/Zn-superoxide dismutase in transfected cells: extenuation of paraquat-mediated cytotoxicity and enhancement of lipid peroxidation. EMBO J., *5:* 615–622, 1986.

45. Ceballos, I., Delabar., J. M., Nicole, A., Lynch, R. E., Hallewell, R. A., and Sinet, P. M. Expression of transfected human CuZnSOD gene in mouse L cells and NS20Y neuroblastoma cells induces enhancement of glutathione peroxidase activity. Biochem. Biophys. Acta, *949:* 5864–5870, 1988.
46. Kelner, M. J., and Bagnell, R. D. Alternations of endogenous glutathione peroxidase, manganese superoxide dismutase, and glutathione transferase activity in cells transfected with copper-zinc superoxide dismutase expression vector: explanation for variation in paraquat resistance. J. Biol. Chem., *265:* 10872–10875, 1990.
47. Kelner, M. J., and Bagnell, R. D., Montoya, M. A., Estes, L., Uglik, S. F., and Cerutti, P. Transfection with human copper-zinc superoxide dismutase induces bi-directional alterations in other antioxidant enzymes, proteins, growth factor response, and paraquat resistance. Free Radical Biol. Med., *18:* 497–506, 1995.
48. Fullerton, H. J., Ditelberg, J. S., Chen, S. F., Sarco, D. P., Chan, P. H., Epstein, C. J., and Ferriero, D. M. Copper/Zinc superoxide dismutase transgenic brain accumulates hydrogen peroxide after perinatal hypoxia ischemia. Ann. Neurol., *44:* 257–364, 1998.
49. Burdon, R. H. Cell proliferation and oxidative stress: Basis for anticancer drugs. Proc. R. Soc. Edinburgh, *99B:* 169–176, 1992.
50. Burdon, R. H., and Gill, V. Cellularly generated active oxygen species and Hela cell proliferation. Free Radical Res. Commun., *19:* 203–213, 1993.
51. Burdon, R. H., Gill, V., and Rice-Evans, C. Cell proliferation and oxidative stress. Free Radical Res. Commun., *7:* 149–159, 1989.
52. Burdon, R. H., Gill, V., and Rice-Evans, C. Oxidative stress and tumor cell proliferation. Free Radical Res. Commun., *11:* 65–76, 1990.
53. Rao, G. N., and Berk, B. C. Active oxygen species stimulate vascular smooth muscle cell growth and proto-oncogene expression. Circ. Res., *70:* 593–599, 1992.
54. Blackburn, R. V., Spitz, D. S., Liu, X., Galoforo, S. S., Sim, J. E., Ridnour, L. A., Chen, J. C., Davis, B. H., Corry, P. M., and Lee, Y. J. Metabolic oxidative stress activates signal transduction and gene expression during glucose deprivation in human tumor cells. Free Radical Biol. Med., *26:* 419–430, 1999.
55. Meister, A. Glutathione deficiency produced by inhibition of its synthesis, and its reversal: application in research and therapy. Pharmacol. Ther., *51:* 155–194, 1991.
56. Meister, A. Glutathione, ascorbate, and cellular protection. Cancer Res., *54:* 1969s–1975s, 1994.
57. Reed, D. J. Regulation of reductive processes by glutathione. Biochem. Pharmacol., *35:* 7–13, 1986.
58. Pickett, C. B., and Lu, A. Y. H. Glutathione *S*-transferase: gene structure, regulation, and biological function. Annu. Rev. Biochem., *58:* 743–764, 1989.
59. Morrow, C. S., and Cowan, K. H. Glutathione *S*-transferase and drug resistance. Cancer Cells, *2:* 15–22, 1990.
60. Droge, W., Schulze-Osthoff, K., Mihm, S., Galter, D., Schenk, H., Eck, H. P., Roth, S., and Gmunder, H. Functions of glutathione and glutathione disulfide in immunology and immunopathology. FASEB J., *8:* 1131–1138, 1994.
61. Kroll, M., Margottin, F., Kohl, A., Renard, P., Durand, H., Concordet, J-P., Bachelerie, F., Arenzana-Seisdedos, F., and Benarous, R. Inducible degradation of IκBα by the proteasome requires interaction with the F-box protein h-βTrCP. J. Biol. Chem., *274:* 7941–7945, 1999.